Determination of the Fe-Ni Phase Diagram below 400 °C

K.B. REUTER, D.B. WILLIAMS, and J.I. GOLDSTEIN

The phase diagram for the Fe-Ni system below 400 °C has been determined experimentally in the composition range from 0 to 52 wt pct Ni using analytical electron microscopy techniques. High spatial resolution X-ray microanalysis and electron diffraction were conducted on the Fe-Ni regions of meteorites. Both stable and metastable phase boundaries were defined. Our phase diagram is consistent with the available theoretical diagram in that firm experimental evidence was found for a miscibility gap and an associated, asymmetrical spinodal decomposition region. The spinodal decomposition resulted in a two-phase, isotropic microstructure, as expected. The miscibility gap is a metastable construction arising from the presence of a tricritical point due to magnetic interactions. Our experimental diagram differs from the theoretical diagram in three ways. First, observations of meteorite structures show that Fe-Ni solid solution containing 4.0 wt pct Ni is in local equilibrium with ordered FeNi containing 51.4 wt pct Ni and not Ni_3Fe as in the theoretical diagram. Second, our miscibility gap below 400 °C, located between 11.7 and 51.9 wt pct Ni at 200 °C, is wider than the calculated miscibility gap, especially at the high Ni end. Third, we also find evidence for an ordered structure around ~25 wt pct Ni. This structure may be either Fe_3Ni or a two-phase structure incorporating ordered FeNi.

I. INTRODUCTION

THERE has been much interest in the Fe-rich portion of the Fe-Ni phase diagram;[1–4] however, this portion of the phase diagram is not well understood at temperatures below 400 °C.[5] Most of the published low temperature phase diagrams are based on speculation,[6–12] or they are calculated thermodynamically.[13,14] Recently, Chuang *et al.*[15] improved the thermodynamic calculations by taking into account the magnetic contribution to the Gibbs free energy for the low Ni, body-centered cubic phase and the high Ni, face-centered cubic phase. Adding the non-magnetic contributions and using the total Gibbs free energies, they calculated the Fe-Ni phase diagram below 900 °C, and a miscibility gap was predicted, associated with a tricritical point at 462 °C and 48.9 wt pct Ni. There is evidence for such a miscibility gap in the Fe-Ni system from experimental observations,[16,6] thermodynamic measurements,[17,18] and thermodynamic calculations.[14] Direct experimental evidence for a miscibility gap has been observed in the Fe-Pd system,[19] a similar system to Fe-Ni.[15]

Little experimental data exist for the Fe-Ni system at low temperatures because of the slow diffusion of Ni in Fe-Ni. For example, at 300 °C, it takes more than 10^4 years for one atomic jump to occur. To overcome this problem, we have examined the structure and chemistry of the metallic phases in iron and stony-iron meteorites. Because meteorites have cooled at a slow rate (~1 °C/10^6 years), low temperature phase transformations can occur. Therefore, the microstructure and microchemistry of the metallic meteorite phases can be used to determine the phase boundaries in the low temperature Fe-Ni phase diagram. Because the phases that form in meteorites at low temperatures are on a submicron scale, analytical electron microscope (AEM) techniques were employed. High spatial resolution X-ray microanalysis using energy dispersive spectrometry (EDS) was used to determine the chemistry, and electron diffraction was used to identify the crystal structures of the various phases. In a parallel investigation, high voltage electron microscopy was used to enhance diffusion in laboratory Fe-Ni alloys permitting *in situ* observation of the ordering transformation that occurs around Fe-50 wt pct Ni. The results of the high voltage work are published in detail in a companion paper,[20] and also are used to shed light on the Fe-Ni phase diagram.

In summary, the objective of this study is to determine experimentally the Fe-Ni phase diagram in the Fe-rich region below 400 °C. The diagram which we produce is consistent with all the phases observed in the Fe-Ni regions of meteorites.[21] We also can compare our phase diagram with the theoretical diagram calculated by Chuang *et al.*,[15] using thermodynamic data. A major point that must be understood is that, while the phase diagram generated by this investigation may contain both metastable and equilibrium phases, true thermodynamic equilibrium below ~400 °C is never reached, even in meteorites which have cooled in the temperature range 700 to 200 °C for more than 10^8 years. This point will be evident from the microchemical data presented in this paper. Therefore, below ~400 °C, the phase diagram (whether calculated or experimentally determined) is strictly a metastable diagram.

II. EXPERIMENTAL PROCEDURES

A. *Meteorite Specimen Preparation*

Appropriate sections of the Dayton, Tazewell, Carlton, and Grant iron meteorites and the Estherville stony iron meteorite were sliced to about 12 mils on a slow speed diamond saw. These slices were polished, etched, examined optically, and areas of interest were electro-discharge machined into 3 mm discs. The discs were thinned on SiC papers to 3 to 4 mils and a Fischione

K.B. REUTER, Senior Materials Scientist, is with Union Carbide Corporation, Tarrytown Technical Center, Tarrytown, NY 10591. D.B. WILLIAMS and J.I. GOLDSTEIN, Professors, are with the Department of Materials Science and Engineering, Lehigh University, Bethlehem, PA 18015.

Manuscript submitted August 14, 1987.

or Struers twin-jet electropolishing unit was used to prepare electron-transparent specimens. The electropolishing units were operated at 105 V with a 2 pct perchloric/98 pct ethanol polishing solution. The temperature of the polishing bath was started at −40 °C and kept below −20 °C. When a thin area did not occur in the region of interest, the specimen was thinned further using a Gatan dual ion miller operated at 6 kV for 10 to 15 minutes.

B. *Chemical Analysis*

Chemical analysis was accomplished using a Philips EM400T AEM equipped with an EDAX EDS detector and a Tracor Northern 2000 multi-channel analyzer. The X-ray quantification was performed using the Cliff-Lorimer ratio method:[22]

$$\frac{C_{Ni}}{C_{Fe}} = k_{NiFe}\frac{I_{Ni}}{I_{Fe}} \qquad [1]$$

where C is the concentration of the element in wt pct; I is the characteristic peak intensity above background; and k_{NiFe} is the proportionality factor termed the Cliff-Lorimer k-factor. The peak intensities above the background for Fe and Ni were calculated using least squares fitting to library standard peaks after the background was removed by digital filtering. To determine k_{NiFe}, at least 18 compositional analyses were obtained from a 45 and 55 wt pct Ni alloy with at least 12,000 counts collected in the smallest peak using windows which included 1.2 times the full width at half the maximum intensity. The precise Ni content of the nominal 45 and 55 wt pct Ni alloys was determined using the electron probe microanalyzer (EPMA). For both alloys, the average k_{NiFe} was calculated as 1.12 with a 1.2 pct error at the 99 pct confidence level.

The low temperature transformation products were analyzed in the five meteorites. The Ni content reported for each transformation product is the average Ni content found in each meteorite at the 95 pct confidence level.

III. RESULTS

A. *Terminology*

The symbols used on the phase diagram and in the following discussion are defined following the teminology used by Chuang *et al.*.[15] The low Ni bcc phase is termed α; γ_1 is the paramagnetic fcc phase; γ_2 is the ferromagnetic fcc phase; γ' is ordered Ni_3Fe; γ'' is ordered FeNi; γ''' is possibly ordered Fe_3Ni; FeNi is the disordered high temperature form of γ''; and α_2 is martensite.

B. *Quantitative X-Ray Analysis and Electron Diffraction*

At high temperatures, the Fe-Ni regions in meteorites are composed of two phases: α, a stable, low Ni bcc phase, and γ_1, a stable, high Ni fcc phase. Below ~400 °C, γ_1 becomes unstable and decomposes to form four regions containing different transformation products. The quantitative X-ray microanalysis data from these four regions form the heart of this paper. A typical bright field (BF) image of an Fe-Ni region in the Tazewell meteorite is shown in Figure 1. The microstructural regions shown are the high temperature, low Ni bcc phase, α, labeled a, followed by the four low temperature transformation products from γ_1: region 1 is γ''; region 2 is the two-phase ($\gamma'' + \alpha_2$) area; region 3 is possibly γ''', and region 4 is α_2. The evidence supporting this classification of the four regions will now be presented and is based on electron diffraction and X-ray microanalysis of the phases present.

The structure and Ni content of each region were determined in the five meteorites, and the results are summarized in Table I. A typical X-ray microanalysis trace showing the Ni variation across the various regions in Figure 1 is shown in Figure 2. The α phase has the lowest Ni content and borders γ'', the phase with the highest Ni content. The average Ni content decreases from the α/γ'' interface through the $\gamma'' + \alpha_2$, γ''', and α_2 regions.

Each of the five microstructural regions was studied in detail, and the structure and chemistry of each was determined as follows: The α phase has a bcc structure and contains 4.0 ± 0.3 wt pct Ni at the interface with γ''. The γ'' phase, region 1 in Figure 1, gives rise to superlattice spots in electron diffraction patterns. The superlattice spots are consistent with ordered FeNi having the $L1_0$ superstructure. The γ'' contains 51.4 ± 1.0 wt pct Ni at the interface with α and decreases to 45.6 ± 1.3 wt pct Ni near the two-phase ($\gamma'' + \alpha_2$) region.

Region 2 in Figure 1 is the two-phase region ($\gamma'' + \alpha_2$), also called the cloudy zone in meteorite terminology because of its appearance in optical micrographs. The γ'' has a globular appearance, and the α_2 shows a honeycomb structure. Figure 3 shows the two phase $\gamma'' + \alpha_2$ region at higher magnification in the Estherville meteorite. Usually the diffraction conditions were adjusted so that γ'' appeared bright and α_2 appeared dark in a bright field TEM image. Electron diffraction shows that glob ular γ'' is the same phase as the single phase region 1; *i.e.*, it is ordered FeNi with the $L1_0$ superstructure. However, the Ni content of the γ'' in this two-phase region is 50.9 ± 1.4 wt pct, which is very close to the value

Fig. 1—Typical BF image of low temperature transformation products in metallic areas of meteorites. Region 1 is γ''; region 2 is $\gamma'' + \alpha_2$; region 3 is possibly γ'''; region 4 is α_2. Also shown is α, labeled a. This specific area was in the Tazewell meteorite.

Table I. Ni Content of the Five Microstructurally Defined Regions in the Metallic Areas of Meteorites

X-Ray Analysis—Location		Wt Pct Ni
α	(at γ'' interface)	4.0 ± 0.3
γ''	(at α interface)	51.4 ± 1.0
	(at $\gamma'' + \alpha_2$ interface)	45.6 ± 1.3
γ''	(in $\gamma'' + \alpha_2$)	50.9 ± 1.4
α_2	(in $\gamma'' + \alpha_2$)	11.7 ± 0.5
	(elsewhere)	<25.8 ± 2.0
γ'''	(at $\gamma'' + \alpha_2$ interface)	28.1 ± 1.8
	(at α_2 interface)	25.8 ± 2.0

of 51.4 ± 1.0 wt pct Ni obtained from the γ'' composition at the γ''/α boundary. The γ'' had the same composition across the width of the $\gamma'' + \alpha_2$ region in the Estherville meteorite. The honeycomb phase surrounding the globular regions is α_2 with a bcc structure and a Ni content of 11.7 ± 0.5 wt pct. The two phases, $\gamma'' + \alpha_2$, are not resolved in the X-ray microanalysis trace in Figure 2 due to electron beam spreading and the very fine scale of the two-phase region in the Tazewell meteorite. As can be seen, the average Ni content decreases across the width of the two phase region.

Region 3 has a Ni content ranging from 28.1 ± 1.8 to 25.8 ± 2.0 wt pct. Superlattice reflections appeared in selected area diffraction patterns (SADPs) from this region, indicating that the structure is ordered and may be either Fe_3Ni[21] or FeNi.[23] The region next to γ''' is α_2, which is termed region 4 in Figure 1. The α_2 is martensite, which has the bcc structure and contains <25 wt pct Ni.

IV. DISCUSSION

From the Ni composition profile in Figure 2, it is easy to see that the meteorite has not reached true thermodynamic equilibrium. If equilibrium had been attained, there would be a constant composition either side of the α/γ'' interface, rather than decreasing Ni content into γ'' as shown. A reasonable interpretation of this profile is that true equilibrium exists only at the α/γ'' interface where α, with 4.0 wt pct Ni, is in contact with ordered γ'' of 51.4 wt pct Ni. Therefore, the *equilibrium* phase diagram at low temperatures should have a simple two-phase field with $\alpha + \gamma''$ present. From this argument, it follows that, as stated in the introduction, all the phases observed in regions 1 to 4 in meteorites that formed below ~400 °C and the phase diagram below 400 °C that we develop as a result, are thermodynamically *metastable*. Given that equilibrium has not been attained in $\sim 10^8$ years of cooling, it is also reasonable to assume that the metastable diagram is the only relevant one to consider in any case.

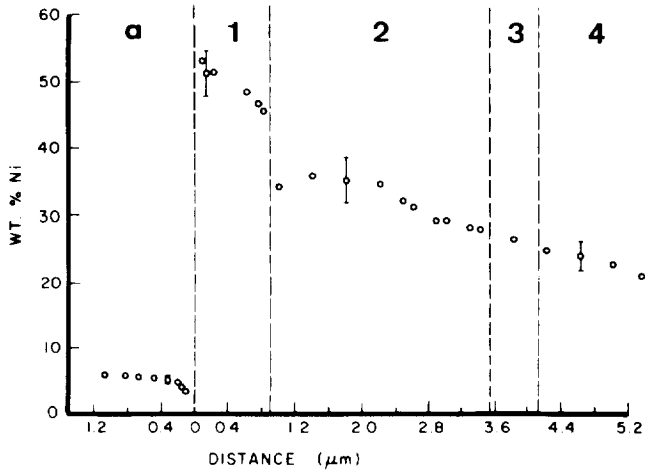

Fig. 2—Typical X-ray microanalysis trace showing the Ni variation across the regions in Figs. 1 and 3.

Fig. 3—Coarse two-phase ($\gamma'' + \alpha_2$) region in the Estherville meteorite. The bright globular γ'' phase contains 50.9 wt pct Ni, and α_2, the surrounding dark phase, contains 11.7 wt pct Ni.

The chemical and structural data described in Section III can be used to generate the stable and metastable phase boundaries below ~400 °C on the Fe-Ni phase diagram, assuming that atomic diffusion essentially ceases at ~200 °C. From the data presented, we have to account for five different phase fields:

(1) ordered FeNi (γ'') with a composition range from 45.6 to 51.4 wt pct Ni;
(2) a two-phase field containing 50.9 wt pct Ni ordered FeNi (γ'') and 11.7 wt pct Ni martensite (α_2);
(3) a single ordered phase field containing an ordered phase with the approximate composition Fe_3Ni;
(4) martensite (α_2) with <25 pct Ni;
(5) bcc α with 4 wt pct Ni.

The easiest way to consider the possible configurations of the various phase fields is to start by examining the theoretical diagram proposed by Chuang *et al.* in Figure 4 and see how this diagram can be modified to account for our experimental observations. Our proposed diagram is shown in Figure 5, and the meteorite data from Table I are placed on the diagram at a temperature of 200 °C. Our arguments to support this diagram are developed in Sections A through D below.

A. *Tricritical Point*

Above ~350 °C Chuang *et al.*'s diagram agrees with previous data from our group based on measurements of Fe-Ni alloys by Romig and Goldstein.[4] The data of Romig and Goldstein are shown as experimental points above ~350 °C. However, Chuang *et al.*[15] introduce a tricritical point at ~450 °C and ~50 wt pct Ni which is discussed in detail in a later paper by Lin and Chang.[24] This tricritical point is based on the rapid change in Curie temperature (T_c) with Ni content and the resultant magnetic contributions to the Gibbs free energy of the fcc high Ni γ_1 phase. Below ~450 °C, this γ_1 phase splits into the low Ni paramagnetic γ_1 and the high Ni ferromagnetic γ_2 phases. Since in meteorites that we studied the local composition does not reach above 50 wt pct Ni at the temperatures where the γ_2 forms, we have no data to contribute on the γ_2 phase field (and also the γ' and other high Ni phase fields). Accordingly, we have left the tricritical point essentially unchanged.

It should be noted that the magnetic contributions to the phase diagram give rise to higher-order phase boundaries; *i.e.*, the dashed lines emanating from the tricritical point in Chuang *et al.*'s diagram are not first-order phase transformation boundaries. Such high-order boundaries and the associated magnetic transformations do not obey simple first-order phase diagram rules such as the phase rule.[24] Therefore, as we have argued above, the dashed lines are metastable phase boundaries below the eutectoid temperature (~400 °C).

B. *The Eutectoid Transformation*

Chuang *et al.*[15] predict a eutectoid transformation at ~40 wt pct Ni and ~400 °C. The proposed eutectoid transformation involves $\gamma_1 \rightarrow \alpha + \gamma_2$. (The $\gamma/\alpha + \gamma$ boundary data of Romig and Goldstein[4] have sufficient errors that the boundary may still be γ_1.) We have presented evidence in support of the eutectoid transformation from $\gamma_1 \rightarrow \alpha + \gamma''$ in a separate paper dealing with meteorite microstructures.[21] In essence, the step in the composition profile between regions 1 and 2 in Figure 2 which occurs at ~40 wt pct Ni can be interpreted as evidence for the eutectoid transformation.

C. *Ordered FeNi (γ'')*

A major discrepancy between Chuang *et al.*'s diagram and our experimental evidence from meteorites is the presence of the FeNi phase. In Chuang *et al.*'s diagram, there is no Fe-50 wt pct Ni single-phase field, but, at 50 wt pct Ni, a two-phase $\alpha + \gamma'$ phase field is predicted. However, the data of Romig and Goldstein[4] indicate that a Fe-50 wt pct Ni phase is present. In addition, our meteorite studies[21,26,27] and the results of many other investigations,[28,29] including studies using radiation to enhance diffusion rates,[30,31] show that a stable, ordered $L1_0$ phase exists. Our measurements at the α/γ'' interface indicate that α of 4 wt pct Ni is in equilibrium with γ'' of 51.4 wt pct Ni at ~200 °C. Accordingly, we propose that a single-phase field for γ'' exists with a measured minimum Ni content of ~51.4 wt pct Ni at 200 °C. In common with results from studies of the γ'' phase, we show a transformation to disordered FeNi above 320 °C.[30] What we cannot deduce from our meteorite data are (a) the maximum Ni content of the γ''/FeNi single-phase field; and (b) how the γ''/FeNi phase field is related to the higher Ni phases γ_2 and γ'. Therefore, the part of the diagram encompassing the $\gamma'' + \gamma_2$ and $\gamma'' + \gamma'$ is speculative, but is close to the calculated diagram of Chuang *et al.*[15] There is no particular reason to have the disordered FeNi phase terminate at the tricritical point, but there also is no reason to terminate the FeNi phase field at a lower temperature. What remains to be clarified is why the γ'' single phase in meteorites persists down to ~46 wt pct Ni, rather than decomposing into $\alpha + \gamma''$ below 51.4 pct, the lower limit of the equilibrium phase. This problem can only be understood when we examine the two-phase $\alpha_2 + \gamma''$ field.

D. *The Two-Phase $\alpha_2 + \gamma''$ Field*

The miscibility gap shown in the diagram calculated by Chuang *et al.* is due to the magnetic Gibbs free energy term for the fcc phase. Note that there is a continuous transition between the Curie temperature and the boundaries of the miscibility gap. This kind of magnetically-induced decomposition can be expected in alloys such as Co-V which have a rapidly changing Curie temperature as a function of composition. Fe-Ni alloys show a similar rapid variation in the Curie temperature with composition.[10]

Below 400 °C, the miscibility gap is continued and is shown as dashed lines representing the metastable phase boundaries. Spinodal boundaries also were calculated by Chuang *et al.* and also are shown as dashed lines with associated cross-hatching on Figure 4. One must be careful to distinguish the spinodal boundaries, which merely denote a change in transformation mechanism, from the metastable two-phase field boundary. Also shown on the diagram are dashed/dotted lines representing the M_s temperature and Curie temperature $\gamma_1(T_c^{\gamma})$.

There is ample evidence in both the meteorite literature[9,10] and the Fe-Ni[32,33] literature for the existence of a miscibility gap and the associated spinodal decomposition region in Fe-Ni alloys containing <50 wt pct Ni. From our experimental evidence, we can draw conclusions about both the miscibility gap and the spinodal decomposition regime. First, we assume that the fine scale two-phase mixture of $\alpha_2 + \gamma''$ arises from spinodal decomposition. The intimate mixing and the obvious high degree of connectivity of the two phases (Figures 1 and 3) argue in favor of a spinodal formation mechanism. Microstructurally, the only argument against a spinodal mechanism is that the two-phase structure does not show the classical variation in the *wavelength* of each phase as a function of composition. It is expected that, if the spinodal region were symmetrical, the γ'' spinodal phase would be large near the γ'' single-phase region, and the α_2 phase would be large at the other extreme of the two-phase region, with the smallest wavelength in the center. In the meteorites (Figure 1), the largest wavelengths appear in the high Ni region near γ'', and the wavelength decreases with decreasing Ni content.

This behavior can be explained if the spinodal region

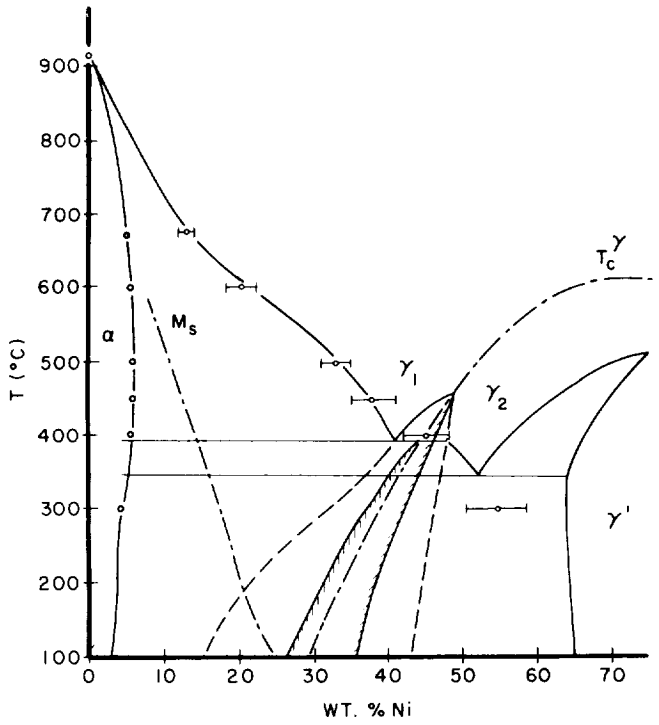

Fig. 4—The Fe-Ni phase diagram calculated by Chuang *et al.*,[15] shown as solid lines, compared with Romig and Goldstein's data,[4] shown as open circles. The dotted/dashed lines show the M_s temperature and the Curie temperature T_C for γ_1 phase. Dashed lines show metastable extension of the miscibility gap from the tricritical point, and the hatched lines delineate the spinodal decomposition region.

is not symmetrical but asymmetrical with a peak close to the maximum Ni content of the two-phase region (~46 pct Ni). As the meteorite cools, the highest Ni regions transform spinodally, followed at lower temperatures by regions of lower Ni content. Consequently, the higher Ni regions have more time to grow and coarsen. Such an asymmetrical spinodal is calculated by Chuang *et al.*, and our microstructural studies are in agreement. The constant value of the composition of the globular and honeycomb phases further attests to the probability that they formed by spinodal decomposition. The average decrease in Ni content across this region is accommodated by a change in the relative *amounts* of the two phases, not changes in their Ni content. From Figure 1, the increasing amount of α_2, with decreasing size of the phases, can be seen clearly.

Our data indicate that the spinodal decomposition occurs over a composition range from ~28 to 46 wt pct Ni (average Ni content variation over the $\alpha_2 + \gamma''$ two-phase region). However, the spinodal *products* form with a composition given by the boundaries of the miscibility gap. Thus, from our data, at 200 °C the miscibility gap boundaries must be at ~11.7 and 50.9 pct Ni, the measured compositions of $\alpha_2 + \gamma''$ in the two-phase structure.

The γ'' formed by spinodal decomposition has a composition (50.9 wt pct Ni) close to, but not the same as, the single-phase γ'' (51.4 wt pct Ni). We cannot distinguish these compositions given the limits of accuracy of X-ray microanalysis in the AEM. However, the γ'' formed by the spinodal mechanism is metastable compared to the single-phase γ'' so we include a dotted line close to the single-phase γ'' boundary to denote the metastable γ'' phase boundary. There is no reason for the metastable and stable γ'' phase boundaries to be close, except that with time one would expect the metastable γ'' to gain in Ni content until it attains the stable composition. Then it would be in equilibrium with α rather than metastable equilibrium with α_2.

Given that FeNi orders below ~320 °C, it is clear that below this temperature any FeNi formed by spinodal decomposition must order rapidly to produce γ''. The fact that α_2 has a Ni content of 11 pct explains why it is martensite. The low Ni miscibility gap boundary must extend to cross the M_s temperature well above 200 °C, so that all the low Ni spinodal product transforms to martensite as the meteorite cools down to 200 °C.

According to the classical theory of spinodal decomposition,[34] alloys outside the spinodal but within the miscibility gap can transform only by a nucleation and growth mechanism. This transformation requires overcoming an activation energy barrier and, therefore, is more difficult to accomplish than spinodal decomposition. Thus, we expect that these regions (*i.e.*, the high Ni region from 46 to 52 wt pct Ni and the low Ni region from 11 to 28 wt pct Ni) are not able to transform spinodally to $\alpha + \gamma''$. These regions then remain initially as supersaturated fcc γ_1 Fe-Ni solid solution.

When the high Ni γ_1 region (46 to 52 wt pct Ni) cools below 320 °C, it orders to the $L1_0$ structure identical to the γ''. (The disorder-order transformation is accomplished with ease because only atomic-level diffusion is required for ordering.) The ordered domains then coarsen as the meteorite cools to 200 °C, after which no further diffusion occurs. Thus, region 1 in the meteorite structure is ordered, supersaturated Fe-Ni that would like to transform to a two-phase structure ($\alpha + \gamma''$) by nucleation and growth but cannot overcome the nucleation barrier. The nucleation barrier is difficult to overcome, because the Ni diffusion kinetics become too slow to permit formation of nuclei greater than the critical size and the critical composition.

A similar argument can be made for the low Ni region (11 to 28 wt pct Ni) of the miscibility gap; *i.e.*, this region remains as supersaturated γ_1 because it cannot nucleate the $\alpha + \gamma''$ stable phases. However, an alternative transformation mode is available for the areas below ~25 pct Ni. When they cool below M_s, they transform to martensite (α_2) by a shear mechanism which requires no thermal activation or solute diffusion and, therefore, is unaffected by the very slow Ni diffusion kinetics.

Further indirect evidence for the position of the spinodal boundary comes from the results of irradiation experiments carried out in the high voltage electron microscope and described in a companion paper.[20] In this work, the electron irradiation was used to enhance the Ni diffusion in order to measure the temperature at which the ordered γ'' phase was formed in laboratory Fe-Ni alloys ranging in Ni content from 32 to 50 wt pct. The critical temperature above which ordering was not observed varied from ~260 to 320 °C over this composition range.[20] According to the evidence from meteorites, irradiating alloys of 32 to 46 wt pct Ni below

the temperature of the spinodal boundary would produce varying amounts of ordered γ'' of ~50 wt pct Ni, by a process of spinodal decomposition, followed by ordering. Irradiating samples at temperatures above the spinodal boundary would not result in the appearance of the ordered phase because, as already discussed, the nucleation barrier could not be overcome. So we propose that measurement of an *apparent* disordering temperature under irradiation in fact corresponds to measurements of the spinodal boundaries. If this is the case, this represents a novel approach to determination of the spinodal position. The irradiation data[20] are used for this purpose, as shown in Figure 5.

In summary, the spinodal region predicted by Chuang *et al.* is consistent in principle with our data but should be expanded to cover the composition range from 28 to 40 wt pct Ni at ~200 °C. The low Ni side of the spinodal region also should be drawn to match the results of irradiation studies of the limit of stability of ordered γ'' (*i.e.*, varying from ~260 °C at 32 wt pct Ni to 320 °C at 46 wt pct Ni). The miscibility gap calculated by Chuang *et al.* also is consistent with our measurements, except that we have broadened the gap so that, at 200 °C, it extends from ~11 pct Ni, well below M_s, to 52 pct Ni, the γ'' boundary.

E. *Supersaturated γ'*

A full account of all the regions observed in meteorites still requires an explanation of region 3 (Figure 1) with a composition of 25 to 28 wt pct Ni. Region 3 is within the defined miscibility gap but outside the spinodal. As described above, this composition region would like to transform by nucleation and growth but cannot do so because of the slow Ni diffusion kinetics. The α_2 encroaches up to ~25 pct Ni which is about the limit of the M_s line at room temperature. The small composition region between 25 and 28 wt pct Ni can neither spinodally decompose nor shear to martensite. However, as discussed elsewhere,[21,23] there is evidence that very faint superlattice spots exist in this region, which could either be due to Fe_3Ni with the $L1_2$ superlattice structure, or FeNi with the $L1_0$ structure. We cannot distinguish between the two phases with the electron microscope. However, preliminary Atom Probe Field Ion Microscopy (APFIM) studies[35] indicate that this region has transformed partially on a scale <5 nm to ordered FeNi with a composition of ~50 wt pct Ni. This result would negate the arguments already presented for the formation of Fe_3Ni. Further work to solve this problem is being carried out.

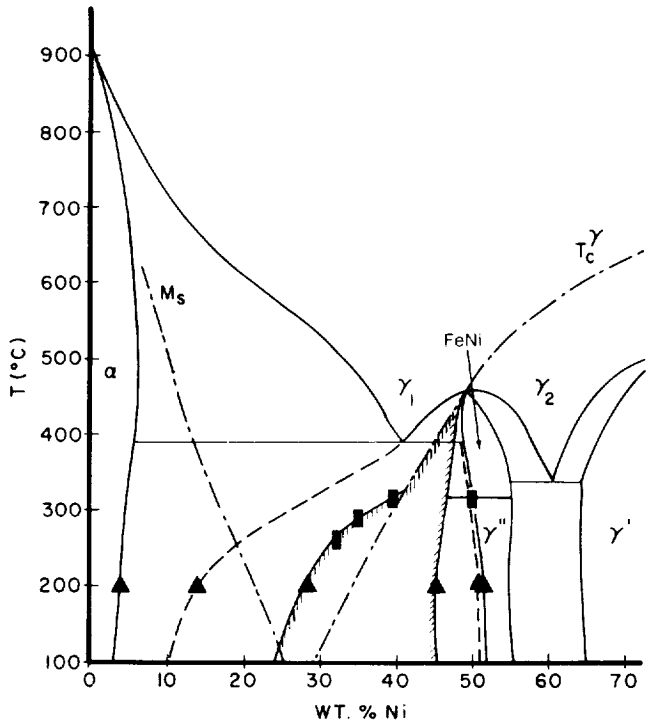

Fig. 5—Phase diagram determined in this study. Experimental data are shown as filled triangles from X-ray microanalysis and as filled rectangles from HVEM. Symbols used are consistent with those of Chuang *et al.*[15] See text for definitions.

F. *α_2-Martensite*

Martensite (α_2) occurs by a shear mechanism whenever the combination of composition and temperature falls below the M_s line in Figure 5. As we have seen, this occurs in two parts of the meteorite structure:

(1) those low Ni regions that form by spinodal decomposition; and
(2) any parts of the microstructure with a composition <~25 wt pct Ni. This value of ~25 wt pct Ni represents the upper limit of stability of α_2 at room temperature.

All these results are summarized in our proposed phase diagram shown in Figure 5. In essence, the diagram accounts for the stable phases above ~400 °C, but below that temperature complete thermodynamic equilibrium is not reached, even in meteorites. The situation is further complicated by the magnetic interactions, which again result in metastable, higher-order lines appearing on the diagram.

G. *Consequences of the Proposed Diagram*

There are several consequences of the proposed diagram that possibly may be tested experimentally to see if the diagram remains self consistent:

(1) If the γ'' between 45 and 51.4 wt pct Ni indeed is metastable with respect to nucleation and growth of the phases defined by the miscibility gap, then electron irradiation of this area in meteorites may help overcome any kinetic barrier to nucleation. However, given the results of irradiation reported in the companion paper, it seems unlikely that this procedure will be successful.
(2) The martensite that forms by shear below M_s should be metastable with respect to the formation of $\alpha + \gamma'''$ or $\alpha + \gamma''$, depending on whether or not Fe_3Ni indeed is a stable phase. It is well known that martensite decomposes in meteorites on a very fine scale, and close examination of the decomposed martensite may well throw light on the γ'''/γ'' problem. This work is being pursued currently.
(3) The γ''' phase is Fe_3Ni or FeNi, but we cannot distinguish these phases by electron diffraction because of spatial resolution limitations. It may be possible to

distinguish between the two phases using higher resolution phase-contrast imaging or a totally different technique such as APFIM. The possibility of using these techniques is being pursued.

(4) It may be possible to deduce more information about the region of the phase diagram $>\sim 52$ wt pct Ni by examining the microstructure and microchemistry of certain (anomalous) meteorites with very high Ni contents which contain Ni_3Fe.[36]

V. CONCLUSIONS

1. The stable phases below ~400 °C in the low Ni region of the Fe-Ni phase diagram are α with 4 wt pct Ni and FeNi with 51.4 wt pct Ni. The FeNi orders to form γ'' below ~320 °C with the $L1_0$ structure.
2. There is a miscibility gap arising at a tricritical point at ~460 °C which extends metastable boundaries below 400 °C. The boundaries of the two-phase miscibility gap at 200 °C comprise α_2 with 11.7 wt pct Ni and γ'' with 50.9 wt pct Ni.
3. Within the miscibility gap, an asymmetrical spinodal decomposition region exists within the composition range 28.1 to 45.6 wt pct Ni at 200 °C.
4. The results of HVEM studies of the order-disorder transformation have been interpreted uniquely in terms of the low Ni side of the spinodal region.
5. Outside the spinodal, but within the miscibility gap, ordered γ'' forms from 45.6 to 50.9 wt pct Ni. Martensite forms below M_s (~25.8 wt pct Ni at room temperature).
6. In the region containing from 25.8 to 28.1 wt pct Ni, there is evidence for ordering. The ordered phase may be Fe_3Ni (γ''') or FeNi.

ACKNOWLEDGMENTS

Many helpful discussions with Professors W.A. Soffa (University of Pittsburgh) and Y.A. Chang (University of Wisconsin-Madison) are acknowledged. The authors also gratefully acknowledge the National Center for Electron Microscopy, Lawrence Berkeley Laboratory, for making the HVEM experiments possible. The work was supported by NASA Grant No. NAG-9-45.

REFERENCES

1. E.A. Owen and A.H. Sully: *Phil. Mag.*, 1939, vol. 27, pp. 614-36.
2. E.A. Owen and Y.H. Liu: *J. Iron Steel Inst.*, 1949, vol. 163, pp. 132-37.
3. J.I. Goldstein and R.E. Ogilvie: *Trans. TMS-AIME*, 1965, vol. 233, pp. 2083-87.
4. A.D. Romig and J.I. Goldstein: *Metall. Trans. A*, 1980, vol. 11A, pp. 1151-59.
5. O. Kubaschewski: *Iron-Binary Phase Diagrams*, Springer-Verlag, New York, NY, 1982, pp. 73-78.
6. A. Chamberod, J. Laugier, and J.M. Penisson: *J. Magn. Magn. Mat.*, 1979, vol. 10, pp. 139-44.
7. J.F. Albertsen, J.M. Knudsen, N.O. Roy-Paulsen, and L. Vistissen: *Physica Scripta*, 1980, vol. 22, p. 171-75.
8. J.I. Goldstein and D.B. Williams: *Proc. Int. Conf. Solid/Solid Phase Transformations*, 1982, TMS-AIME, Warrendale, PA, pp. 715-19.
9. R.A. Jago, P.E. Clark, and P.L. Rossiter: *Phys. Stat. Sol. (a)*, 1982, vol. 74, pp. 247-54.
10. J.F. Albertsen, H.P. Nielsen, and V.F. Buchwald: *Physica Scripta*, 1983, vol. 27, pp. 314-20.
11. A.A. Yarnell: *Meteoritika* (in Russian), 1983, vol. 42, pp. 66-71.
12. P.L. Rossiter and R.A. Jago: *Mat. Res. Soc. Symp. Proc.*, T. Tsakalokos, ed., Elsevier, 1984, pp. 407-11.
13. L. Kaufman and H. Nesor: *Z. Metallkd.*, 1973, vol. 54, pp. 249-57.
14. P.L. Rossiter and P.J. Lawrence: *Phil. Mag. A*, 1984, vol. 49, pp. 536-46.
15. Y.Y. Chuang, Y.A. Chang, R. Schmid, and J.C. Lin: *Metall. Trans. A*, 1986, vol. 17A, pp. 1361-72.
16. A. Chamberod, M. Roth, and L. Billard: *J. Magn. Magn. Mat.*, 1978, vol. 7, pp. 101-03.
17. O. Kubaschewski, K.H. Geiger, and K. Hack: *Z. Metallkd.*, 1977, vol. 68, pp. 337-41.
18. Y. Tanji, Y. Nakagawa, L.Y. Saito, K. Nishimura, and K. Nakatsuka: *Phys. Stat. Sol. (a)*, 1979, vol. 56, pp. 513-19.
19. E. Raub, H. Beeskow, and O. Loebich: *Z. Metallkd.* (in German), 1963, vol. 54, pp. 549-52.
20. K.B. Reuter, D.B. Williams, and J.I. Goldstein: *Metall. Trans. A*, 1989, vol. 20A, pp. 711-18.
21. K.B. Reuter, D.B. Williams, and J.I. Goldstein: *Geochimica et Cosmochimica Acta*, 1988, vol. 52, pp. 617-26.
22. G. Cliff and G.W. Lorimer: *J. Microsc.*, 1975, vol. 103, pp. 203-07.
23. K.B. Reuter, D.B. Williams, and J.I. Goldstein: *Proc. 45th Annual Meeting of the Electron Microscopy Society of America*, G.W. Bailey, ed., San Francisco Press, San Francisco, CA, 1987, pp. 216-17.
24. J-C. Lin and Y.A. Chang: *Metall. Trans. A*, 1988, vol. 19A, pp. 441-46.
25. D.E. Laughlin and W.A. Soffa: in *Physical Properties and Thermodynamic Behavior of Minerals*, E.K.H. Salje, ed., D. Reidel Pub. Co., Dordrecht, Holland, NATO ASI Series C, 1988, vol. 225, pp. 213-64.
26. K.B. Reuter: *Proc. 43rd Annual Mtg. Electron Microscopy Society of America*, G.W. Bailey, ed., San Francisco Press, San Franscisco, CA, 1985, pp. 338-39.
27. S. Mehta, P.M. Novotny, D.B. Williams, and J.I. Goldstein: *Nature*, 1980, vol. 284, pp. 151-53.
28. R.S. Clarke and E.R.D. Scott: *Amer. Mineral.*, 1980, vol. 65, pp. 624-30.
29. J.F. Petersen, M. Aydin, and J.M. Knudson: *Phys. Lett.*, 1977, vol. 62A, pp. 192-94.
30. J. Paulevé, D. Dautreppe, J. Laugier, and L. Néel: *J. de Physique* (in French), 1962, vol. 23, pp. 841-43.
31. A. Chamberod, J. Laugier, and J.M. Penisson: *J. Magn. Magn. Mater.*, 1979, vol. 10, pp. 139-44.
32. P.L. Rossiter and P.J. Lawrence: *Phil. Mag. A*, 1984, vol. 49, pp. 535-46.
33. J.R.C. Guimaraes and J.C. Sayne: *Metall. Trans.*, 1971, vol. 2, pp. 2063-65.
34. J.W. Cahn: *Trans. AIME*, 1968, vol. 242, pp. 166-80.
35. M.K. Miller and K.F. Russell: *J. de Physique*, 1988, vol. 44, in press.
36. J. Danon, M. Christophe Michel-Lévy, K. Keil, G.B. Gomez, B.R.B. Scorzelli, and I. Souza Azevedo: *1981 Meteorites*, vol. 16, p. 305.